A modified method of characteristics and its application in forward and inversion simulations of underwater explosion

Chengjiao Zhang,[a] Xiaojie Li, and Chenchen Yang
Department of Engineering Mechanics, Dalian University of Technology, Dalian, 116024, China

(Received 10 January 2016; accepted 19 July 2016; published online 26 July 2016)

This paper introduces a modified method of characteristics and its application in forward and inversion simulations of underwater explosion. Compared with standard method of characteristics which is appropriate to homoentripic flow problem, the modified method can be also used to deal with isentropic flow problem such as underwater explosion. Underwater explosion of spherical TNT and composition B explosives are simulated by using the modified method, respectively. Peak pressures and flow field pressures are obtained, and they are coincident with those from empirical formulas. The comparison demonstrates the modified is feasible and reliable in underwater explosion simulation. Based on the modified method, inverse difference schemes and inverse method are introduced. Combined with the modified, the inverse schemes can be used to deal with gas-water interface inversion of underwater explosion. Inversion simulations of underwater explosion of the explosives are performed in water, and equation of state (EOS) of detonation product is not needed. The peak pressures from the forward simulations are provided as boundary conditions in the inversion simulations. Inversion interfaces are obtained and they are mainly in good agreement with those from the forward simulations in near field. The comparison indicates the inverse method and the inverse difference schemes are reliable and reasonable in interface inversion simulation.
[http://dx.doi.org/10.1063/1.4960116]

I. INTRODUCTION

Gas bubble pulsation is an important research subject in underwater explosion of spherical explosive, and it has been widely studied. After explosive converts into gas, bubble starts expansion and its pressure falls. When the bubble boundary pressure falls to that of surrounding water, it would over expand because of inertia. And the bubble would cease expansion and be in contraction phase pressed by surrounding water. During the contraction process, the bubble pressure would rise gradually. When the contraction process cease, the bubble would expand again. The expansion and contraction process would repeat several times in bubble pulsation. Every expansion and contraction process would cause pressure variation and form a pressure wave which would transmit into water and form a shock wave. Among the shock waves, only the first one plays an important role in damage and therefore it has research value.

Experiments and numerical simulations are the main research methods in the subject. Many researchers have studied characteristics of underwater explosion by means of underwater explosion experiment, most of which were carried out in small-scale.[1–3] In the experiments, explosive ball is placed in center of transparent water containers which is convenient for streak camera to record photographs. In the bubble pulsation stage, variation of gas-water interface is captured by streak

[a]Electronic mail: zhangchj@mail.dlut.edu.cn.

camera and recorded in photos. However, it is not accurate to obtain all experimental results according to small-scale experiments. Explosive charge can affect detonation performance of some explosives. Detonation parameters of the explosives including detonation pressure and detonation velocity change with explosive charge. For industrial ammonium nitrate explosive, its detonation velocity would increase from 2000m/s to 4600m/s with the increment of explosive charge diameter from 20 mm to 150 mm. Another example is aluminized PBXW-115 military explosive whose detonation velocity would increase from 5100m/s to 6000m/s with the increment of explosive charge diameter from 40 mm to 200 mm.[4] The difference in detonation velocities would affect detonation performance significantly. It indicates that experiment cannot be only limited in small-scale. Moreover, streak camera can only capture bubble expansion process. While other important properties such as pressure and density of gas-water interface are really difficult to be measured with current instruments. Thus the experimental method still has limitations.

Numerical simulation plays an increasingly important role with development of numerical method and compute technology. It has important value in testifying reliability of experiment and predicting experimental result. Therefore numerical simulation makes up for the limitations. Many numerical methods have been applied in underwater explosion simulations. Corresponding simulated results including properties of shock wave, bubble and flow field can be obtained and some of them are difficult to be measured in experiment. Many researchers have performed underwater explosion simulations to study bubble pulsation.[5–8] Most underwater explosion simulations base on forward problem, and detonation product EOS parameters are of importance and necessity in the forward simulations.[9–12] Standard method of characteristics is a classical calculation method and has clear physical significance. In applying the standard method, simulation relies on right-traveling and left-traveling waves which indicate propagation direction of small disturbance. Inverse calculation can be also performed along right-traveling and left-traveling waves and therefore the standard method of characteristics is applicable to inversion problem. Moreover, in applying the standard method to discontinuity problem such as underwater explosion, artificial viscosity is not needed in simulations, which reduces the effect of non-objective intervention.[13–17] However, the standard method of characteristics is only applicable to homoentropic flow problem. Underwater explosion as a typical isentropic flow problem cannot be solved with the standard method.

In this paper, a modified method of characteristics and its application in forward and inversion simulation of underwater explosion are introduced.[18] Compared with the standard method, the modified method has a wider application range and can be applied to isentropic flow problems. This paper introduces forward simulations of underwater explosion of spherical TNT and composition B explosives first. Peak pressures and flow field pressures are obtained and the simulated results are coincident with those from empirical formulas in acceptable accuracy, which indicates the modified method is feasible and reliable in forward simulation of underwater explosion.[19–21] Based on the modified method, inverse difference schemes and inverse method are introduced and applied in inversion simulations of underwater explosion. The inversion simulations are only performed in water and thus detonation product EOS is not needed. The underwater shock waves from the forward simulations are taken as known conditions in the inversion simulations. Properties of gas-water interfaces including position and physical parameters are solved and they are in good agreement with the forward ones in near field. The comparison demonstrates that the inverse method and the inverse difference schemes are feasible and reliable. Because detonation product EOS is not used in inversion simulation, the inverse schemes can be also combined with parameters of shock wave measured in experiment to confirm gas-water interface properties for explosive whose detonation parameters are unknown.

II. BASIC EQUATIONS OF THE MODIFIED METHOD OF CHARACTERISTICS

Based on one-dimensional compressible Euler equations ignoring heat conduction and fluid viscosity, basic equations of the modified method can be derived as follow.[18]

$$\begin{cases} \left(\frac{\mathrm{d}r}{\mathrm{d}t}\right)_{\mathrm{I}} = u + C \\ \left(\frac{\mathrm{d}p}{\mathrm{d}t}\right)_{\mathrm{I}} + \rho C\left(\frac{\mathrm{d}u}{\mathrm{d}t}\right)_{\mathrm{I}} - \left(\frac{\partial p}{\partial e}\right)_{\rho}\left(\frac{T\mathrm{d}S}{\mathrm{d}t}\right)_{\mathrm{III}} + \frac{\mathrm{N}\rho C^2 u}{r} = 0 \end{cases}, \tag{1}$$

and

$$\begin{cases} \left(\frac{\mathrm{d}r}{\mathrm{d}t}\right)_{\mathrm{II}} = u - C \\ \left(\frac{\mathrm{d}p}{\mathrm{d}t}\right)_{\mathrm{II}} - \rho C\left(\frac{\mathrm{d}u}{\mathrm{d}t}\right)_{\mathrm{II}} - \left(\frac{\partial p}{\partial e}\right)_{\rho}\left(\frac{T\mathrm{d}S}{\mathrm{d}t}\right)_{\mathrm{III}} + \frac{\mathrm{N}\rho C^2 u}{r} = 0 \end{cases}, \tag{2}$$

where ρ, u, e and p are density, velocity, internal energy, and pressure of fluid, respectively, and the subscript I, II and III denote right-traveling waves, left-traveling waves and particle path lines, respectively. t and r represent time and distance to original point, respectively. S is entropy and C is adiabatic sound velocity. $N = 0, 1, 2$ indicates planar flow, radial flow, and spherically symmetrical flow, respectively. The entropy change terms in equations (1)~(2) indicate the modified method can be applied in isentropic flow problem. A third family characteristic equation, consisting of particle path line equation and energy conservation equation, is introduced

$$\begin{cases} (\mathrm{d}r/dt)_{\mathrm{III}} = u \\ (\mathrm{d}Q)_{\mathrm{III}} = [\mathrm{d}e + p\mathrm{d}\,(1/\rho)]_{\mathrm{III}} \end{cases}, \tag{3}$$

The equations (1)~(3) constitute the basic equations of the modified.

III. EQUATIONS FOR ONE-DIMENSIONAL SPHERICAL SYMMETRIC UNDERWATER EXPLOSION

In this paper, forward and inversion simulations of underwater explosion of spherical composition B and TNT explosives are performed by using the modified method. The two kind explosives belong to ideal explosive which has stable detonation properties. Underwater explosion experiments of the two explosives were performed and experimental data were obtained. Empirical formulas based on the experimental data have been summarized and they can be used to verify the reliability of the modified method. In the simulations, the effects of gravity and bubble migration are neglected. Chapman-Jouguet (C-J) model of detonation product is applied. It is assumed that the surrounding water is infinite, and hence the simulations are not affected by reflected waves from boundary.

A. Basic characteristics equations for underwater explosion

In underwater explosion of spherical explosive, strength of underwater shock wave reduces quickly in near field, and corresponding fluid entropy productions are quite different. Thus it is an isentropic flow behind shock wave. The fluid pressures behind shock wave unload along different adiabatic isentropes and entropy productions of particles are zero. In underwater explosion, the basic physical and state characteristic equations of right-traveling and left-traveling waves can be simplified, respectively.

$$\begin{cases} \left(\frac{\mathrm{d}r}{\mathrm{d}t}\right)_{\mathrm{I}} = u + C \\ \left(\frac{\mathrm{d}p}{\mathrm{d}t}\right)_{\mathrm{I}} + \rho C\left(\frac{\mathrm{d}u}{\mathrm{d}t}\right)_{\mathrm{I}} + \frac{N\rho C^2 u}{r} = 0 \end{cases}, \tag{4}$$

$$\begin{cases} \left(\dfrac{\mathrm{d}r}{dt}\right)_{\mathrm{II}} = u - C \\ \left(\dfrac{\mathrm{d}p}{\mathrm{d}t}\right)_{\mathrm{II}} - \rho C\left(\dfrac{\mathrm{d}u}{\mathrm{d}t}\right)_{\mathrm{II}} + \dfrac{N\rho C^2 u}{r} = 0 \end{cases}. \tag{5}$$

And the third characteristic equation can be derived

$$\begin{cases} \left(\dfrac{\mathrm{d}r}{\mathrm{d}t}\right)_{\mathrm{III}} = u \\ \left[\mathrm{d}e + p\mathrm{d}\left(\dfrac{1}{\rho}\right)\right]_{\mathrm{III}} = 0 \end{cases}. \tag{6}$$

The equations (4)~(6) are basic characteristic equations for underwater explosion. Rankine-Hugoniot relations are used to deal with underwater shock wave, as below

$$\begin{cases} \rho_0 (u_{\mathrm{S}} - u_0) = \rho_{\mathrm{H}} (u_{\mathrm{S}} - u_{\mathrm{H}}) \\ p_{\mathrm{H}} - p_0 = \rho_0 (u_{\mathrm{S}} - u_0)(u_{\mathrm{H}} - u_0), \\ e_{\mathrm{H}} - e_0 = (p_{\mathrm{H}} + p_0)(v_0 - v_{\mathrm{H}})/2 \end{cases} \tag{7}$$

where the subscripts 0 and H denote undisturbed and being disturbed state by shock wave, respectively, u_S is shock wave velocity, and v is specific volume, $v = 1/\rho_0$.

B. Equation of state for water

In this work, a polynomial EOS of water is used

$$\begin{cases} p = A_1\mu + A_2\mu^2 + A_3\mu^3 + (\mathrm{B}_0 + \mathrm{B}_1\mu)\rho_0 e_{\mathrm{m}} & \mu \geq 0 \\ p = T_1\mu + T_2\mu^2 + \mathrm{B}_0\rho_0 e_{\mathrm{m}} & \mu < 0 \end{cases}, \tag{8}$$

where ρ_0 is reference density, $\rho_0 = 1.0$ g/cm^3. $\mu = \rho/\rho_0 - 1$, $\mu > 0$ denotes compression state and $\mu < 0$ denotes tension state. e_{M} is specific internal energy per unit mass. Other parameters are $A_1 = 2.2$ GPa, $A_2 = 9.54$ GPa, $A_3 = 14.57$ GPa, $T_1 = 2.2$ GPa, $T_2 = 0$, $\mathrm{B}_0 = 0.28$, and $\mathrm{B}_1 = 0.28$. The Hugoniot data of the polynomial EOS agree with experimental data well, and the EOS can satisfy most simulations of dynamic impacts below 40.0 GPa.[18,22]

C. Equation of state for products

The pressure-volume-energy behavior of detonation products is modeled with the standard Jones-Wilkins-Lee (JWL) EOS

$$p = A\left(1 - \frac{\omega}{R_1\mathrm{V}}\right)e^{-R_1\mathrm{V}} + B\left(1 - \frac{\omega}{R_2\mathrm{V}}\right)e^{-R_2\mathrm{V}} + \frac{\omega E}{\mathrm{V}}, \tag{9}$$

where E is specific internal energy per unit mass, and for a certain explosive V is the specific volume of detonation products over the specific volume of undetonated explosive. JWL EOS parameters of TNT and composition B explosives are shown in Table I.[11]

TABLE I. JWL EOS parameters of TNT and composition B explosives.

Explosive	ρ_0(g/cm^3)	D(cm/μs)	p_{H}(GPa)	A(GPa)	B(GPa)	R_1	R_2	ω
TNT	1.63	0.693	21.0	373.77	3.747	4.15	0.9	0.35
Comp. B	1.717	0.798	29.5	524.2	7.678	4.2	1.1	0.34

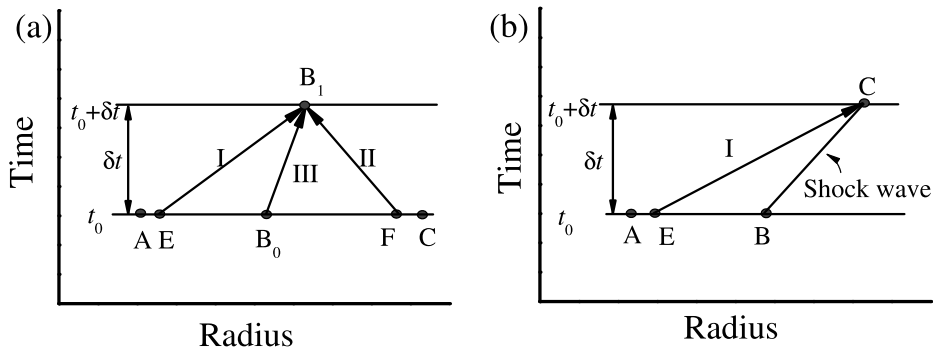

FIG. 1. (a). The schematic diagram of fixed-time difference scheme for forward simulations. The symbols I and II denote right-traveling and left-traveling waves, respectively. The symbol III denotes a particle path line. (b). The schematic diagram of difference scheme of shockwave for forward simulations.

IV. FORWARD SIMULATIONS OF UNDERWATER EXPLOSION OF SPHERICAL EXPLOSIVE

In this work, corresponding codes are developed based on the modified method and they are used to simulate underwater explosion of spherical explosive. To verify the reliability of the modified method and the codes, simulated results are compared with empirical formulas.

A. Difference schemes in forward simulation

The basic difference scheme is fixed-time technique and shown in Fig. 1(a). Properties of mesh points at constant time line t_0 are known. δt is time increment. The properties of point B_1 at constant time line $t_0 + \delta t$ is to be solved. Points B_1 and B_0 are at the same path line. Path line is used to confirm the position of point B_1. And state characteristic equations of right-traveling and left-traveling waves combined with material's EOS are used to solve properties of point B_1. Specifically, a right-traveling wave passed through point B_1 has an intersection (point E) with the time line $t = t_0$, and properties of point E are calculated from interpolation between those of points A and B_0. Similarly, a point F can be found at the time line $t = t_0$ to satisfy the requirement that points F and B_1 are at the same left-traveling wave. Properties of point F are obtained from interpolation between those of points B_0 and C. Based on points E, B_0 and F, properties of point B_1 are determined using the state characteristics in equations (4)~(5) and material's EOS. The first iteration is completed as above. All mesh points in domain of influence can be solved layer by layer. High-order interpolation can be applied for better accurate results. In applying the updated results from the latest iteration, multiple iterations can be performed for more accurate results.

As shown in Fig. 1(b), difference scheme for shock wave is similar to the basic scheme. Fig. 1(b) shows there is a shock discontinuity which divides the flow field into two parts, and the shock discontinuity can be considered as a boundary. The shock wave and the left part behind the shock wave are continuous on physical properties, while the shock wave and the other part are discontinuous. Therefore, only right-traveling waves from the left part can be used to calculate the shock wave. Points B and C are disturbed by the shock wave at time t_0 and t_1, respectively. δt is time increment. Point C is to be solved. Shock wave propagation trajectory are used to confirm the position of point C. And state characteristic equation of right-traveling wave and Hugoniot relations are used to calculate properties of point C. The solution of point E is similar to that in Fig. 1(a). Points C and E are at the same right-traveling wave, and properties of point E can be confirmed from the interpolation between those at points A and B. Based on the points E and B, properties of point C are determined by equations (4), (7) and material's EOS.

B. Solid wall boundary and gas-water interface in simulation

In the forward simulations, explosive center is a singular point with unbounded values which can abort calculations. To avoid the affect, spherical explosives are modeled as a hollow sphere with

inner radius 0.2 cm. The inner sphere surface as initial detonation surface is defined as a solid wall boundary after initial detonation.

It is important to capture interface of different materials in simulation. The modified method has the superiority in capturing materials' interface. In this work, two grid points are defined at gas-water interface. One denotes water while the other denotes detonation product. The two points share the same pressure and particle velocity. According to the difference scheme in Fig. 1(a), combined equations (4)~(5) and materials' EOS, properties of interface points can be calculated.

C. Empirical formulas of underwater explosion of spherical explosive

1. Empirical formula of composition B explosive

Chi and Ma designed and conducted a underwater explosion experiment in a semi-flat ball water pool with a diameter of 80 m and a depth of 11 m.[21] A spherical composition B explosive weighting 1.0 kg was placed in 5.0 m underwater. Peak pressures of underwater shockwave were measured with manganin gauge and PVDF gauge during the scaled distance from 1 to 400. They summarized an empirical formula based on the measured peak pressures

$$p_{\mathrm{m}} = 18.33(R_0/R)^{1.07} \exp\left[-2.78 + 2.20\,(R_0/R) + 0.58(R_0/R)^2\right]. \tag{10}$$

2. Empirical formula of TNT explosive

R.H. Cole summarized a series of non-contact underwater explosion empirical formulas in his work. One of them is a peak pressure empirical formula for TNT explosive.[1] B.V. Zamyshlyaev improved the empirical formula[19]

$$p_{\mathrm{m}} = \begin{cases} 4.41 \times 10^7 \left(W^{1/3}/R\right)^{1.5} & 6 < (R/R_0) < 12 \\ 5.24 \times 10^7 \left(W^{1/3}/R\right)^{1.13} & 12 \le (R/R_0) \le 240 \end{cases}, \tag{11}$$

where p_{m} is peak pressure, W is mass of TNT explosive, R_0 is radius of spherical explosive, R is the distance from sphere center to a gauge point. The pressure versus time relation at a certain scaled distance is

$$p(t) = \begin{cases} p_{\mathrm{m}} \exp\left(-t/\theta\right) & t < \theta \\ 0.368 p_{\mathrm{m}} \left(\theta/t\right)\left[1 - \left(t/t_{\mathrm{p}}\right)^{1.5}\right] & \theta \le t \le t_1 \end{cases}, \tag{12}$$

where θ and t_{p} are a time constant and positive time period of shock wave, respectively. Their expressions are as follow

$$\theta = \begin{cases} 0.45 R_0 \left(R/R_0\right)^{0.45} \cdot 10^{-3} & R/R_0 \le 30 \\ 3.5\left(R_0/c\right)\sqrt{\lg\left(R/R_0\right) - 0.9} & R/R_0 > 30 \end{cases}, \tag{13}$$

$$t_{\mathrm{p}} = \left(\frac{850}{\bar{\mathrm{p}}_0^{0.85}} - \frac{20}{\bar{\mathrm{p}}_0^{1/3}} + \mathrm{m}\right)\frac{R_0}{c}, \tag{14}$$

The t_1 and p^* in expression are as follow

$$\frac{t_1}{\left(t_1 + 5.2 - \mathrm{m}\right)^{0.87}} = 4.9 \times 10^5 \left(\frac{p_{\mathrm{m}}}{p_{\mathrm{atm}}}\right)\frac{\theta c R}{R_0^2}, \tag{15}$$

$$p^* = \frac{7.173 \times 10^8}{\left(R/R_0\right)\left(ct/R_0 + 5.2 - \mathrm{m}\right)^{0.87}}, \tag{16}$$

where p_{atm} is standard atmospheric pressure, c is sound velocity of water. $\bar{\mathrm{p}}_0$ and m are dimensionless parameters, and their expressions are

$$\mathrm{m} = 11.4 - 10.6/\left(R/R_0\right)^{0.13} + 1.51/\left(R/R_0\right)^{1.26}, \tag{17}$$

$$\bar{p}_0 = (p_{atm} + \rho g H_0) / p_{atm}, \tag{18}$$

where H_0 is depth of explosive in water.

D. Forward simulations and result discussions

Underwater explosion of spherical TNT and composition B explosives are simulated with the modified method and AUTODYN software, respectively. The calculated results including peak pressure and flow pressure are compared with empirical formulas which are based on experimental data. The experimental data could be affected by experimental instrument accuracy and external disturbance. In the AUTODYN simulations, artificial viscosity is required to be introduced in discontinuity problems and shock wave spreads into narrow region in which flow variables change rapidly but continuously. Discontinuity problems are turned into continuous ones in fact. Simulated results are affected directly by artificial viscosity coefficients whose selection has no objective standard, and therefore non-objective intervention can be introduced into simulations obviously. The modified method does not need to introduce artificial viscosity in calculations. Calculated results from the modified method are theoretical solution, and errors can be only numerical errors from process of numerical calculation. Therefore the calculated results from the modified method are objective.

1. Underwater explosion simulations from AUTODYN software

The simulations are modeled with one-dimensional axial symmetry wedge model.[23] The wedge model has an inner radius of 0.2 cm, and outer radii of 259 cm and 210 cm for composition B and TNT explosives, respectively. In the AUTODYN simulations, artificial viscosity is introduced to smooth nonphysical saw-toothed oscillations. And quadratic and linear viscosity coefficients are 1.0 and 0.67, respectively.[13]

2. Simulations of composition B explosive

As shown in Fig. 2(a), peak pressure curves are compared in exponential coordinate system. The curve of the modified method attenuates exponentially and fits well with the empirical formula curve. And its error percentages are shown in Fig. 2(b). The initial peak pressure from the empirical

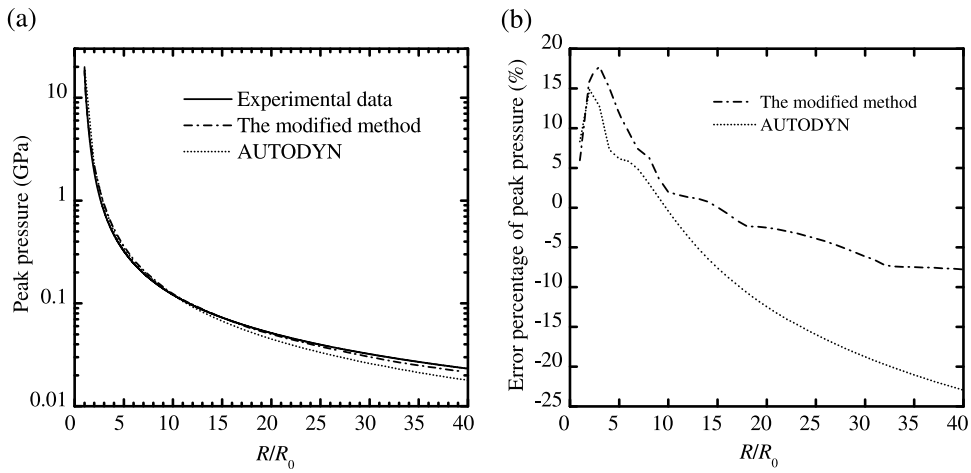

FIG. 2. Analysis of peak pressures in underwater explosion of spherical composition B explosive. (a) Comparisons of peak pressures during scaled distances of 1 to 40. (b) Error percentage of peak pressure analysis. The expression of error percentage is $(p\text{-}p_{\text{empirical formula}})/p_{\text{empirical formula}} * 100\%$.

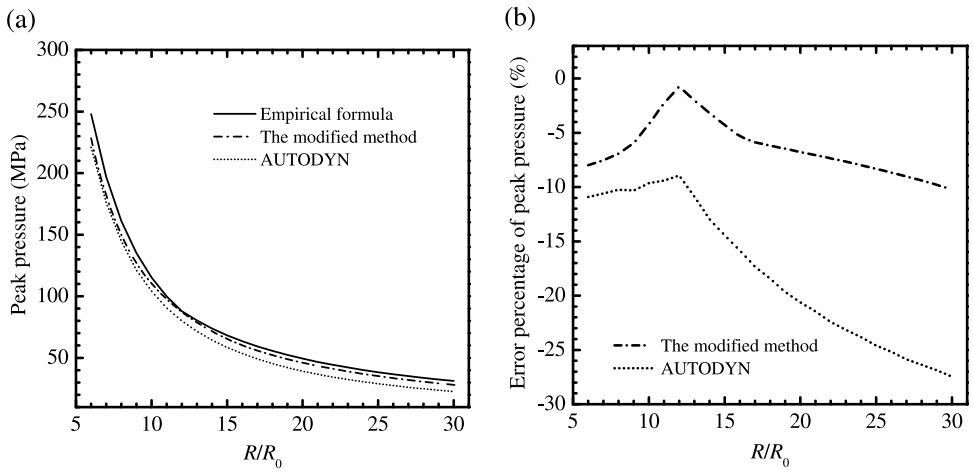

FIG. 3. Analysis of peak pressures in underwater explosion of spherical TNT explosive. (a) Comparisons of peak pressure during the scaled distances of 6 to 30. (b) Error percentage of peak pressure analysis. The expression of error percentage is $(p_{\text{the modified method}} - p_{\text{empirical formula}})/p_{\text{empirical formula}} * 100\%$.

formula, the modified method and AUTODYN are 18.33GPa, 19.41GPa and 19.86GPa, respectively. With shock wave propagation, the error percentages from the modified method increase rapidly first, then decrease gradually and stabilized at -7.75% finally. The largest error percentage is 17.76% at the position of 3.0 charge radii. Affected by artificial viscosity, the error percentages from AUTODYN enlarge continuously. Peak pressure from the modified method is more accurate in near and medium field compared with that from AUTODYN.

3. Simulations of TNT explosive

In equation (12), the smallest applicable scope of the empirical formulas is 6 charge radii. There is no appropriate data to compare within the scope of 6 charge radii. As shown in Fig. 3(a), all simulated peak pressures attenuates exponentially and are coincident with those from the empirical formulas. In Fig. 3(b), error percentage curves first decrease and then rise with shock wave propagation. The error percentages from the modified are less than 10% basically. The smallest percentage error is -0.73% at the position of 12 charge radii, while the largest percentage error is -10.21% at the position of 30 charge radii. The error percentages from AUTODYN are much larger than those from the modified with shock wave propagation. The comparison indicates the peak pressures from the modified method are more coincident with empirical formula compared with those from AUTODYN.

As shown in Fig. 4, based on the pressure-time history formulas in equation (13), pressure-time history curves are compared at the position of 6 and 15 charge radii, respectively. And the curves are coincident with those of the empirical formulas mainly. At the 15 charge radii, the peak pressure from AUTODYN is smaller than that from the modified method and empirical formula significantly.

According to the comparisons shown in Figs. 2~4, simulations from the modified method agree well with the results of the empirical formulas in acceptable accuracy. The comparison results demonstrate that the modified method and the forward difference schemes are correct and reliable, and they can be used to obtain accurate results in underwater explosion simulation.

V. APPLICATIONS OF THE MODIFIED METHOD IN INVERSE PROBLEM

In this work, inverse difference schemes for inverse problem are also introduced and applied in inversion simulation of underwater explosion. Based on the shock waves from the forward simulations, inversion simulations of underwater explosion are performed with the inverse schemes. Both trajectory and physical properties of gas-water interfaces are obtained from the inversion

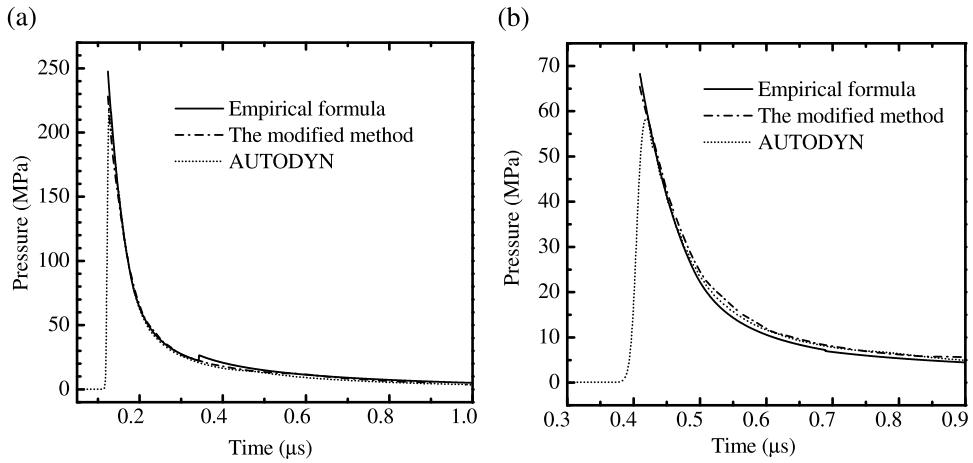

FIG. 4. Comparison of pressure-time curve of TNT explosive. (a) Pressure-time curves at the position of 6 charge radii. (b) Pressure-time curves at the position of 15 charge radii.

simulations, and they are compared with the forward ones to verify the reliability of the inverse schemes.

A. Inverse difference schemes for inversion simulation

Inverse difference schemes are different from the forward ones, and they are not the fixed-time technique which is not appropriate for inverse problem, as shown in Fig. 5. Point A is to be solved. Particle path lines and right-traveling waves are combined to determine time-space coordinate position of point A, and state characteristic equations of right-traveling and left-traveling waves and water EOS are combined to solve physical properties of point A.

In Fig. 5(a), Points B, H, and E are known. There must be a point A at path line EA which intersects with a right-traveling wave AB. A left-traveling wave passed through point A must have an intersection (point C) with either path line BH or right-traveling wave EH. Properties of point C are obtained from the interpolation between those of points E and H or between those of points B and H. According to points B, C, and E, properties of point A are can be calculated with the state characteristics in equations (4)~(5) and water's EOS.

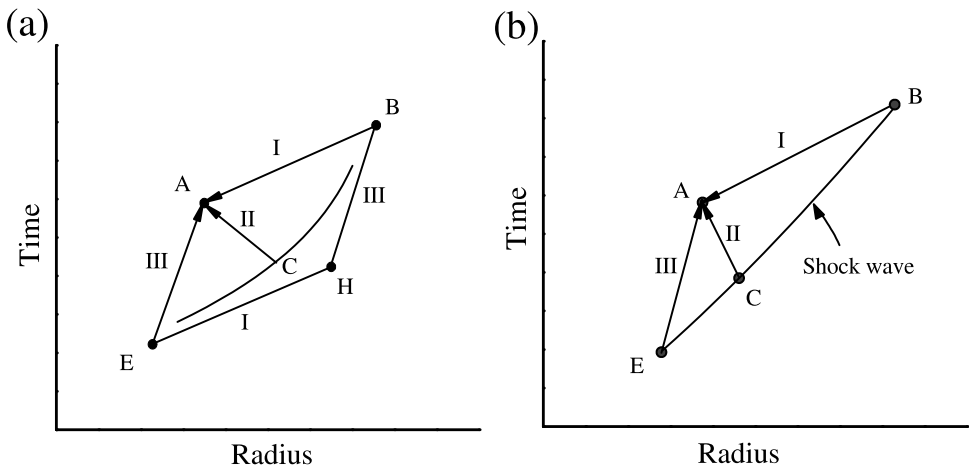

FIG. 5. (a) Schematic diagram of basic difference scheme for inversion simulations in physical plane. (b) The schematic diagram of difference scheme of shock wave for inversion simulations.

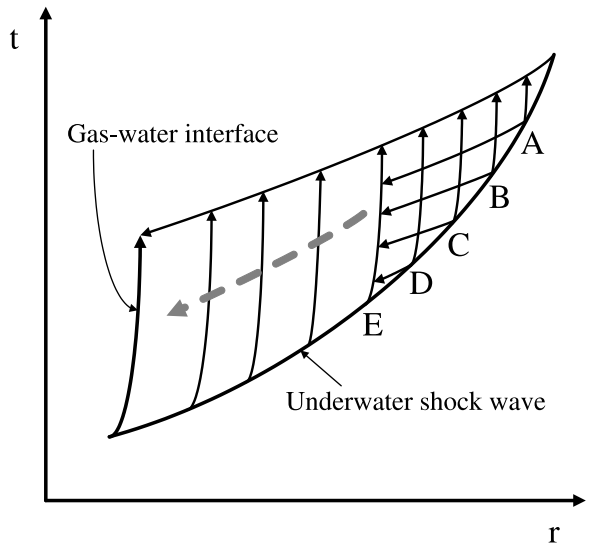

FIG. 6. Schematic diagram of inverse difference grids in physical plane.

As shown in Fig. 5(b), a shock wave passed through points B and E in order. Properties of the two points are known. In physical plane, path line EA has an intersection (point A) with a right-traveling wave passed through point B. And a left-traveling wave passed through point A must has an intersection (point C) with the shock wave BE. Properties of point C are determined by equation (7) and water's EOS. According to points B, C, and E, properties of point A can be solved with the state characteristics in equations (4)~(5) and water's EOS.

Right-traveling waves and path lines intersect and form difference grids in physical plane, as shown in Fig. 6. Underwater shock wave as a boundary is known in inversion simulation. And the inversion simulation should be performed along path lines in sequence which is from path line A to gas-water interface. The specific calculation process is as follows. A point at path line A can be calculated in applying the inverse difference scheme from Fig. 5(b). The calculated point at path line A can be used to solve adjacent path line B as known conditions. And then, in applying the inverse schemes of Figs. 5(a) and 5(b), points at path line B can be calculated one by one along time sequence. The calculated points at path line B are used to solve its adjacent points at path line C. In this way, path lines C, D, and E can be solved one after another, and finally gas-water interface can be solved along the dash line direction shown in Fig. 6.

B. Boundary condition in inversion simulation

Underwater shock wave as boundary condition is known in inversion simulation. In experiments, peak pressures are easier to be measured compared with particle velocity and density. Peak pressures of underwater shock wave can be measured with different kinds of pressure sensors and summarized as empirical formula.[1,21] In applying the measured peak pressures, all other properties of the shock wave can be solved with water's EOS and Hugoniot relations. Combined equation (8) with the energy conservation equation in equation (7), Hugoniot pressure of water can be derived

$$p_{\mathrm{H}} = \frac{2\left(\mathrm{A}_1\mu + \mathrm{A}_2\mu^2 + \mathrm{A}_3\mu^3\right)}{\left[2 - \mu\left(\mathrm{B}_0 + \mathrm{B}_1\mu\right)\right]/\left(\mu + 1\right)}. \tag{19}$$

According to equation (19), peak pressure is a function with the single independent variable μ, and thus μ can be solved with the measured p_H. Combined equations (7), (9), shock wave velocity can be derived

$$u_{\mathrm{S}} = \sqrt{\frac{p_{\mathrm{H}}}{\rho_0} \cdot \frac{\mu + 1}{\mu}}. \tag{20}$$

Thus based on equations (19), (20), other shock wave properties can be solved with the Hugoniot relations. Taking the derivative of pressure with respect to density from equation (8), adiabatic sound velocity can be derived

$$C_S = \sqrt{\frac{1}{\rho_0}(A_1 + 2A_2\mu + 3A_3\mu^2) + B_1 e_m + (B_0 + B_1\mu)\frac{p}{\rho^2}}, \tag{21}$$

where C_S is adiabatic sound velocity. Thus all shock wave properties used in inversion simulation can be solved, and they can be applied as boundary condition.

C. Inversion simulations and discussions

Based on the modified method and inverse difference schemes, two inversion simulations are performed. The shock waves from the forward simulations above are taken as boundary conditions in the inversion simulations. Gas-water interfaces are calculated. To testify the reliability of the inverse schemes, the inversion interfaces are compared with those from the forward simulations.

The positions of the inversion interfaces are coincident with the forward ones in near field, which is shown in Figs. 7(a) and 8(a). The inversion interfaces expand slightly slower compared with the forward ones. In Figs. 7(b) and 8(b), the inversion interface pressures are attenuate exponentially, and they are coincident with the interface pressure from the forward simulations. The initial interface pressures of composition B and TNT explosives are 19.42GPa and 14.52GPa, respectively. And the smallest inversion interface pressures are 0.831GPa and 0.708GPa, respectively.

The inversion interface pressures at the same scaled distance are greater than the forward ones generally. The detailed pressure comparisons of composition B and TNT explosives are shown in Figs. 9 and 10, respectively. In Fig. 9, the largest pressure error is 147.9 MPa at 1.4 charge radii, and the largest pressure error percentage is 20.13% at 1.45 charge radii. In Fig. 10, the largest pressure error is 91.2 MPa at 1.4 charge radii, and the largest pressure error percentage is 14.78% at the same position. Both pressure error and their percentage increase with scaled distance. Although pressure errors do not change much, the corresponding pressure error percentages increase with scaled distance continuously. Two reasons can result in the increasing pressure errors. The first one is the change of difference schemes in forward and inversion simulations. The fixed-time schemes are used in the forward simulations, and it is different from the inverse ones. The difference in schemes could cause calculation error. The other reason is error accumulation in the simulations.

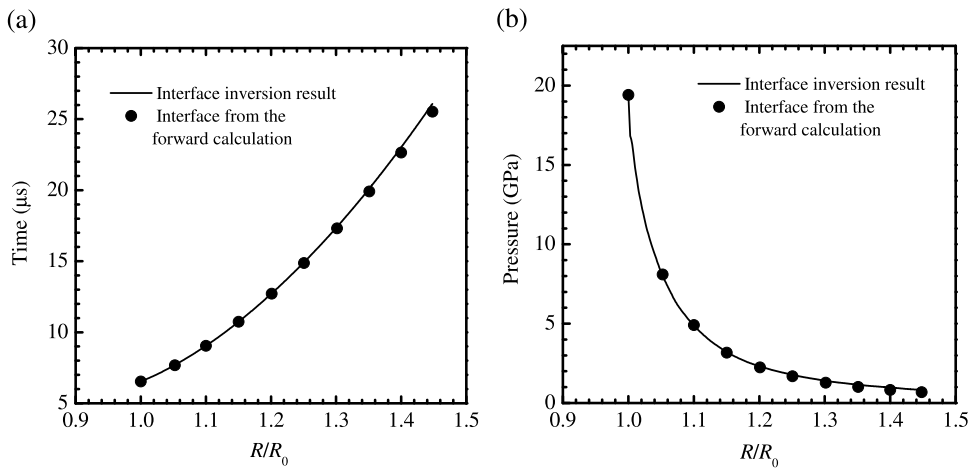

FIG. 7. Inversion interface of composition B explosive. (a) Comparison of gas-water interface position from the inversion and forward simulations. (b) Comparison of gas-water interface pressure from the inversion and forward simulations.

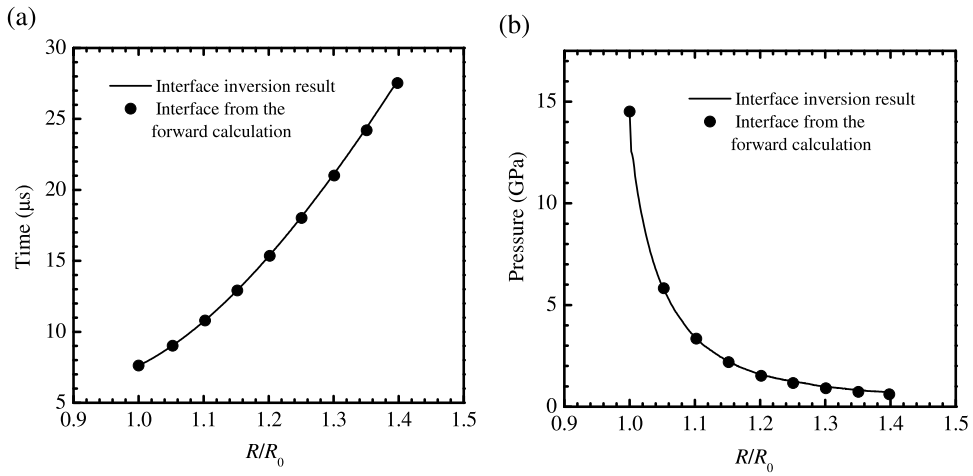

FIG. 8. Inversion interface of TNT explosive. (a) Comparison of gas-water interface position from the inversion and forward simulations. (b) Comparison of gas-water interface pressure from the inversion and forward simulations.

Better interpolation method can be applied to reduce the calculation error. The increasing pressure error percentage is due to the rapid decline of inversion interface pressure.

The inversion simulations end when the inversion interfaces expand to 1.4 and 1.45 charge radii, respectively. In underwater explosion simulations of spherical explosive, right-traveling waves would be dense at interface and sparse at shock wave, as shown in Fig. 11(a). If the points of shock wave are evenly distributed in inversion simulation, the calculation in low pressure region of interface would cost more shock wave points than that in high pressure and medium pressure regions. Thus it would cost much more time in the low pressure region compared with the high pressure and medium pressure regions. It indicates that computational efficiency decline quickly in low pressure region. What is more, the inverse difference scheme shown in Fig. 5(a) is regular in high pressure region, and the inversion simulation can be performed. However, the inverse scheme would be distorted easily in low pressure region because of right-traveling waves which become more and more dense, and thus the right-traveling waves are more likely to intersect. The grids

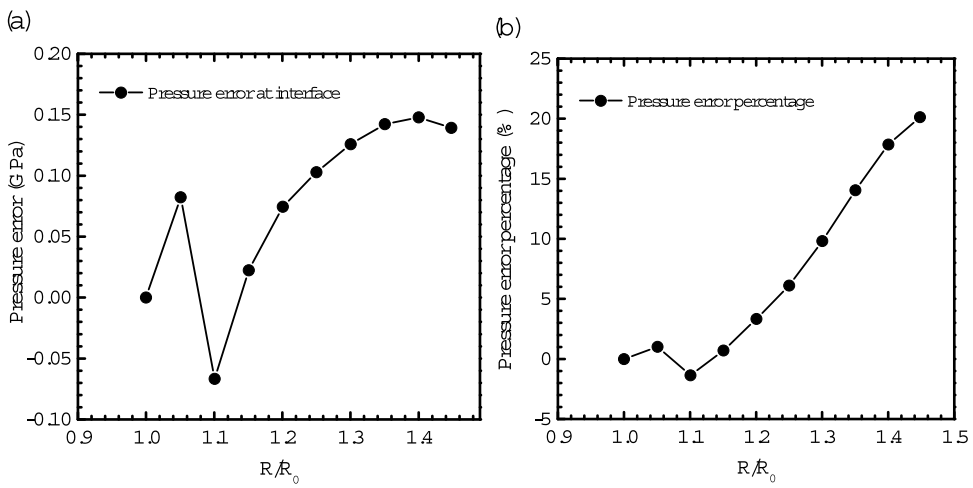

FIG. 9. Interface pressure comparison of composition B explosive. (a) Pressure error is defined as pressure difference between the inversion interface pressure and the forward one, and it is expressed as the formula "$p_{Error} = p_{Inversion\ result} - p_{Forward\ result}$". (b) Pressure error percentage is defined as the ratio between pressure error and interface pressure from the forward calculation, and it can be expressed as the formula "$p_{Error\ percentage} = (p_{Inversion\ result} - p_{Forward\ result})/p_{Forward\ result} \times 100\%$".

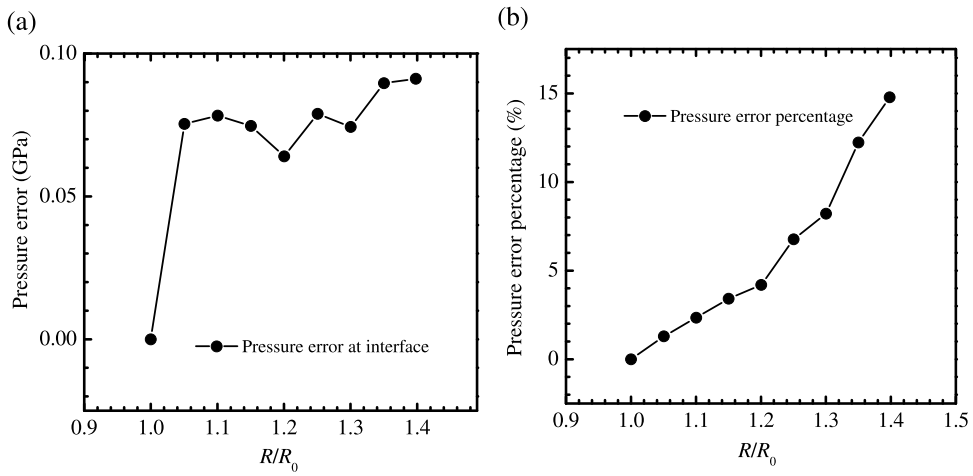

FIG. 10. Interface pressure comparison of TNT explosive. (a) Pressure error is defined as pressure difference between the inversion interface pressure and the forward one, and it is expressed as the formula "$p_{\text{Error}} = p_{\text{Inversion result}} - p_{\text{Forward result}}$". (b) Pressure error percentage is defined as the ratio between pressure error and interface pressure from the forward calculation, and it can be expressed as the formula "$p_{\text{Error percentage}} = (p_{\text{Inversion result}} - p_{\text{Forward result}})/p_{\text{Forward result}} \times 100\%$".

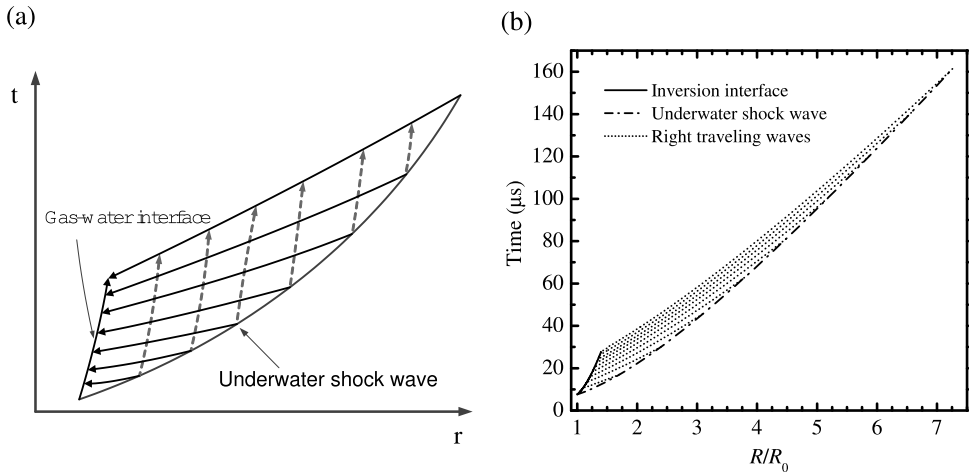

FIG. 11. Right-traveling waves which start from gas-water interface and end at underwater shock wave. (a) Schematic diagram. (b) Right-traveling waves of the inversion simulation of spherical TNT explosive.

distortion and intersection can result in decrease of computational efficiency and precision. It can be summarized that the inversion method is more applicable to interface inversion in high pressure and medium pressure regions. The right-traveling waves from the inversion simulation of TNT explosive is shown in Fig. 11(b).

VI. CONCLUSIONS

In this paper, the modified method of characteristics is introduced and applied in the forward and inversion simulations of underwater explosion of spherical explosive. TNT and composition B explosives are used in the simulations. In the forward simulations, the calculated peak pressure and pressure of flow are coincident with those from empirical formulas in acceptable accuracy. The comparisons indicate that the modified method is reliable in forward simulation of underwater explosion of spherical explosive. And then the inverse difference schemes for inverse problems are introduced. Inversion method is described in detail. In applying the peak pressures of shock wave from the forward simulations, the inversion simulations are performed in water, and gas-water

interfaces are obtained. The inversion interfaces are coincident with the forward ones mainly. The comparison indicates that the inverse difference schemes and inversion method are reliable and accurate in near field and they can be applied to inversion simulation of underwater explosion. Gas-water interface can be solved with the inversion method. According to the continuous condition, pressure and velocity of detonation product equal those of water at gas-water interface. Based on the pressure and velocity of detonation products, further inversion search can be made to study detonation parameters of detonation product.

ACKNOWLEDGMENTS

The authors gratefully acknowledge the support from National Natural Science Foundation of China (Grant nos. 11272081).

[1] R. H. Cole, *Underwater explosions* (Princeton University Press, Princeton, 1948), Vol. 41.
[2] J. Li and J. L. Rong, Ocean Engineering **38**, 1861 (2011).
[3] C. F. Hung and J. J. Hwangfu, Journal of Fluid Mechanics **651**, 55 (2010).
[4] J. P. Lu and D. L. Kennedy, *Modeling of PBXW-115 Using Kinetic CHEETAH and DYNA Codes* (1996).
[5] J. B. Keller and Kolodner II, Journal of Applied Physics **27**, 1152 (1956).
[6] A. M. Zhang, X. L. Yao, and X. B. Yu, Journal of Sound and Vibration **311**, 1196 (2008).
[7] G. Barras, M. Souli, N. Aquelet, and N. Couty, Ocean Engineering **41**, 53 (2012).
[8] Y. L. Liu, A. M. Zhang, and Z. L. Tian, Ocean Engineering **75**, 46 (2014).
[9] C. Y. Chen, J. H. Shiuan, and I. F. Lan, Propellants Explosives Pyrotechnics **19**, 9 (1994).
[10] E. Lee, H. Hornig, and J. Kury, *ADIABATIC EXPANSION OF HIGH EXPLOSIVE DETONATION PRODUCTS* (1968).
[11] B. M. Dobratz, "LLNL explosives handbook: properties of chemical explosives and explosives and explosive simulants," Report No. UCRL-52997 United StatesFri Feb 08 00:54:47 EST 2008NTIS, PC A23/MF A01.LLNL; ERA-06-019173; EDB-81-058557English (1981).
[12] E. Lee, M. Finger, and W. Collins, "JWL equation of state coefficients for high explosives," Report No. UCID–16189 United States10.2172/4479737Thu Mar 24 08:53:59 EDT 2011Dep. NTISLLNL; NSA-28-007802English (1973).
[13] H. Huang, Q. J. Jiao, J. X. Nie, and J. F. Qin, Journal of Energetic Materials **29**, 292 (2011).
[14] M. Nejad-Asghar, A. R. Khesali, and J. Soltani, Astrophysics and Space Science **313**, 425 (2008).
[15] E. J. Caramana, M. J. Shashkov, and P. P. Whalen, Journal of Computational Physics **144**, 70 (1998).
[16] H. Abbassi, F. Mashayek, and G. B. Jacobs, Computers & Fluids **98**, 152 (2014).
[17] S. Siegler and H. Riffert, Astrophysical Journal **531**, 1053 (2000).
[18] X. Li, C. Zhang, X. Wang, and X. Hu, Journal of Applied Physics **115**, 104905 (2014).
[19] B.V. Zamyshlyaev, "Dynamic loads in underwater explosion," (1973).
[20] J. Qiankun and D. Gangyi, International Journal of Impact Engineering **38**, 558 (2011).
[21] J. C. Chi and B. Ma, Chinese Journal of High Pressure Physics **13**, 199 (1999).
[22] S. P. Marsh, *LASL shock Hugoniot data* (Univ of California Press, 1980), Vol. 5.
[23] A. AUTODYN, *Interactive Non-Linear Dynamic Analysis Software, Version 12, User's Manual* (2009).